Ultrafast dynamics of superconducting K_3C_{60} and Rb_3C_{60}

S. B. Fleischer,* B. Pevzner,† and D. J. Dougherty‡
Department of Electrical Engineering and Computer Science, Massachusetts Institute of Technology, Cambridge, Massachusetts 02139-4307
and Research Laboratory for Electronics, Massachusetts Institute of Technology, Cambridge, Massachusetts 02139-4307

H. J. Zeiger
Department of Physics, Massachusetts Institute of Technology, Cambridge, Massachusetts 02139-4307

G. Dresselhaus
Francis Bitter Magnet Laboratory, Massachusetts Institute of Technology, Cambridge, Massachusetts 02139-4307

M. S. Dresselhaus and E. P. Ippen
Department of Electrical Engineering and Computer Science and Department of Physics, Massachusetts Institute of Technology, Cambridge, Massachusetts 02139-4307

A. F. Hebard§
Bell Laboratories, Lucent Technologies, Murray Hill, New Jersey 07974
(Received 17 May 1999; revised manuscript received 9 November 1999)

We report the results of a detailed experimental and theoretical study of the ultrafast relaxation processes in superconducting K_3C_{60} and Rb_3C_{60} films. Room temperature pump-probe spectra were obtained for different pump and probe wavelengths. Low-temperature measurements through the phase transition temperature T_c were performed to monitor the quasiparticle dynamics in the superconducting state. For comparison we performed measurements on $YBa_2Cu_3O_7$ under similar conditions. An intuitive model is presented to explain the temperature and wavelength dependence of our experimental results for both the superconducting and normal phases.

I. INTRODUCTION

The discovery of superconductivity in the fcc M_3C_{60} phase has inspired considerable experimental and theoretical research on these materials.[1–4] Two pump-probe studies on alkali-metal-doped C_{60} films have already been reported. Dynamic transmission spectra of C_{60} and its rubidium intercalant Rb_xC_{60} (where x was reported to be near 2) obtained under high laser excitation density were published by Brorson *et al.*[5] An exact doping level of $x=3$, however, is important to ensure that the samples are metallic, as determined by temperature-dependent conductivity measurements that show metallic behavior only for a narrow range of x near 3 and hopping conductivity otherwise.[6] A low-excitation-density femtosecond pump-probe study of the two important intercalation compounds K_3C_{60} and Rb_3C_{60} was reported by Fleischer *et al.*[7,8] Both studies[5,7,8] were based on the colliding-pulse mode-locked dye laser and therefore were limited to a fixed wavelength of about 625 nm or 2 eV photon energy, and both studies report only room-temperature measurements. Furthermore, the first study[5] was performed on underdoped nonmetallic samples that do not show the superconducting phase transition. Thus far no systematic wavelength-dependent or temperature-dependent pump-probe study of the superconducting M_3C_{60} compounds has been reported.

On the other hand, a good deal of work has been done on the transient response of high-T_c and metallic superconductors to impulsive optical excitation with subpicosecond light pulses, since such measurements give important information on the dynamics of Cooper pair breaking and recombination. A variety of results have been reported in the literature ranging from nanosecond excitation in aluminum[9,10] to femtosecond studies on $YBa_2Cu_3O_7$ (YBCO) and other high-temperature superconductors.[11–31] Terahertz generation in thin superconducting films,[32] current-biased superconducting antennas,[33] and current-biased bridges[34] have also been used to study the optically induced quasiparticle dynamics. Changes in the amplitude and dephasing of optically excited coherent phonons in the normal and superconducting phases of YBCO were investigated by Albrecht *et al.*[12]

In this paper we report on optical pump-probe experiments in well characterized films of K_3C_{60} and Rb_3C_{60} which have been shown to have superconducting transition temperatures of 18 K and 28 K, respectively.[35] A systematic study was made of the variation of the ultrafast dynamics with wavelength, polarization, power, fluence, and temperature. The modeling we have employed in explaining the results for M_3C_{60} is discussed in Sec. V.

It has been found experimentally that these alkali-metal-doped fullerites (M_3C_{60}) behave in many ways like BCS superconductors.[36] Since K_3C_{60} and Rb_3C_{60} have rather high transition temperatures, they offer the unique possibility of performing femtosecond optical pump-probe experiments through the transition temperature. Similar studies have been reported on high-T_c superconductors,[11–31,37] but since the mechanism of the transition in such materials is not well

understood, it is of some interest to compare those studies with our alkali-metal-doped C_{60} results. We briefly discuss such a comparison in Sec. IV B. A more detailed comparison will be reported elsewhere.[38]

II. SAMPLE PREPARATION

The doped films of K_3C_{60} and Rb_3C_{60} used for our pump-probe measurements were optically thick, homogeneous, polycrystalline films deposited on quartz, glass, and sapphire substrates, with a typical film thickness of 5000 Å. They are the same films used in our room-temperature observation of coherent phonons in these materials.[7]

Crystalline C_{60} films were grown using sublimation in a gradient furnace. An evacuated quartz tube was placed into a furnace having two temperature zones, a hot ($\sim 400\,^{\circ}$C) central zone for the sublimation of C_{60} and a cooler ($\sim 200\,^{\circ}$C) end zone for the placement of the substrate onto which C_{60} vapor was condensed. Typical 5000-Å-thick films were grown in approximately 12 hours in a dynamic vacuum of 6×10^{-7} Torr. X-ray diffraction data[39] suggest that the structural coherence of these crystalline C_{60} films approaches that seen in a single crystal (>5000 Å). The long-range order seen in these films can be contrasted with the short structural coherence length (<100 Å) seen in C_{60} films grown by vapor sublimation onto room-temperature substrates and in bulk powder samples.[40]

The crystalline C_{60} films, together with an alkali-metal (K or Rb) dispenser and a porous getter, were then placed in a glass-enclosed assembly for alkali-metal doping and subsequent measurements of transport and optical properties. Platinum leads epoxied in a Van der Pauw configuration to Ag pads on the C_{60}-coated substrate served the dual role of supporting the sample and providing a means to monitor its *in situ* resistivity. The alkali-metal dispenser and porous getter were outgassed (by applying electric currents) in vacuum, after which the assembly was backfilled with He to a pressure of 0.10 Torr and sealed off.

Doping was accomplished by placing the entire assembly in an oven set for temperatures in the range 150–250 °C and then alternately exposing the sample to a flux from the alkali-metal source followed by an anneal for several hours at about 200 °C. The conductivity of the film was monitored continuously with a four-point probe during the doping and annealing steps. The sequence of doping and annealing steps was repeated until no further increase in the conductivity could be obtained. It is important not to overdope the sample past the resistance minimum ($x=3$ for M_3C_{60}, where $M=\mathrm{K,Rb}$).[35] Because of slow M atom diffusion and the necessity of avoiding an overshoot of the resistivity minimum, the length of time to reach the resistance minimum after a succession of exposure-anneal cycles was typically one week or more.

The doped samples were encapsulated in glass ampoules under helium atmosphere. To maintain a high-purity inert environment, an activated beryllium getter was sealed off with the sample. Electrical feedthroughs allowed us to measure low-temperature transport properties and to verify the doping level without ever breaking the inert gas environment. The superconducting transition temperatures were measured and were found to be 18 K and 28 K for K_3C_{60} and Rb_3C_{60}, respectively, in good agreement with literature values.[36]

To prepare the samples for low-temperature measurements, the ampoules were broken and the samples were transferred into an ultrahigh vacuum continuous-flow cold-finger cryostat. To ensure sample integrity, this transfer was undertaken in an argon glove box with 0.1 ppm to 1 ppm oxygen concentration, which was continuously monitored during the sample transfer with an oxygen trace analyzer (0.1 ppm sensitivity). The UHV cryostat was then sealed off and pumped down. To reduce the initial outgassing and to obtain a fast ''pump-down,'' the cryostat was kept at a 10^{-9} Torr vacuum level prior to the sample transfer, and the vacuum was broken only inside the glovebox. We obtained a vacuum of 2×10^{-7} Torr after 15 minutes of pumping, and the pressure dropped to 10^{-8} Torr after 4 hours. To maintain the vacuum, an ion pump was added as an integral part of the cryostat and an ultimate pressure in the low 10^{-9} Torr range was reached after 48 hours.

The optically thick M_3C_{60} films, not the Pyrex substrates, were pressed against indium foil (99.99% pure) to ensure proper thermal anchoring, and the pump-probe measurements were done in reflection and through the back of the substrate. This was necessary because the low thermal conductivity of glass would otherwise result in a locally heated spot. With a Pyrex substrate, the temperature increase underneath the focused laser beam was estimated to be ≈ 50 K, which would raise the local sample temperature above T_c. Here we have assumed an absorbed optical power of 1 mW focused to a 100 μm spot and a thermal conductivity of 1.5×10^{-1} W/mK for glass at 20 K.[41] The indium foil largely eliminates this heating. Furthermore, the indium foil also protected the film from direct exposure to the UHV, thus reducing possible outgassing and an associated reduction of the doping level. To further minimize the chance of sample contamination, we performed our pump-probe measurements immediately after the sample transfer.

III. ROOM-TEMPERATURE EXPERIMENTS

A. Optics

The tuning ranges for Ti:sapphire lasers[42] and optical parametric oscillators[43] (OPO's) are roughly limited to 25% of their center wavelength. To study the frequency dependence of the room-temperature ultrafast dynamics in the K_3C_{60} and Rb_3C_{60} samples, we therefore performed pump-probe studies at widely separated wavelengths utilizing different, but synchronized, laser resonators and/or second harmonic generation. A series of pump-probe experiments with a fixed wavelength pump beam of 775 nm (1.6 eV) and three different probe wavelengths of 650 nm (1.9 eV), 1.3 μm (0.96 eV), and 2 μm (0.64 eV) was performed for both the Rb_3C_{60} and K_3C_{60} samples. The time resolution for all these measurements was better than 200 fs, given a deconvolved pulse width of less than 120 fs for both pump and probe. The pump for this series of experiments was obtained straight from a Ti:sapphire laser oscillator, while the probe was the second harmonic of the signal at 650 nm, the signal at 1.3 μm, and the idler at 2 μm of a synchronously pumped OPO.

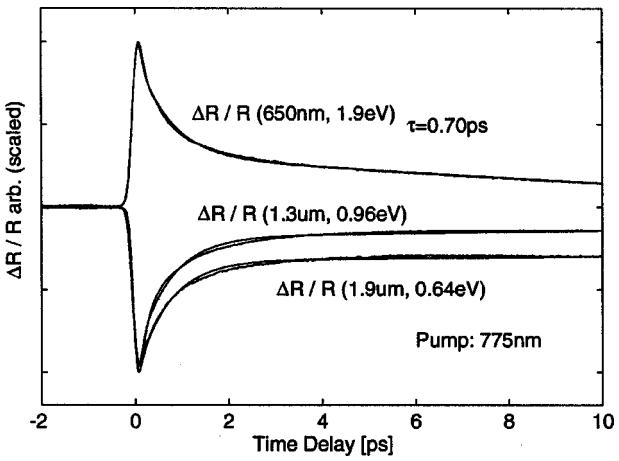

FIG. 1. Pump-probe time-resolved differential reflectance obtained for K_3C_{60} at room temperature for a pump excitation at 775 nm (1.60 eV) and various probe wavelengths smaller than and greater than that of the pump.

B. Experimental results

Figure 1 shows the room-temperature time-resolved differential reflectance $\Delta R(t)/R$ obtained for K_3C_{60} as a function of delay time between pump and probe for our three probe frequencies. Figure 2 shows the corresponding response for Rb_3C_{60}, plotted in the same way for comparison. An approximate average power of 5 mW was used for the pump and probe for all wavelengths. Since the pump was double chopped at 2 kHz and at about 7 MHz, the peak power for the pump was roughly four times higher than that for the probe, so that the probe could be considered as much lower in intensity. The beams were focused with a 75 mm or 100 mm focal length lens down to a spot size in the approximate range 50 μm to 100 μm, resulting in an excitation density of ≈ 1 $\mu J\,cm^{-2}$. All traces in Figs. 1 and 2 were normalized to their peak values to allow better visualization and comparison. The observed $t=0$ changes $\Delta R(0)/R$ in the transient response show a considerable increase toward longer wavelengths. The optical density of the Rb_3C_{60} film was low enough to allow both reflection and transmission measurements to be carried out. Aside from the opposite sign, the $\Delta T/T$ and $\Delta R(t)/R$ data show the same time signature, and no dependence on the polarization (s or p) was found.[8]

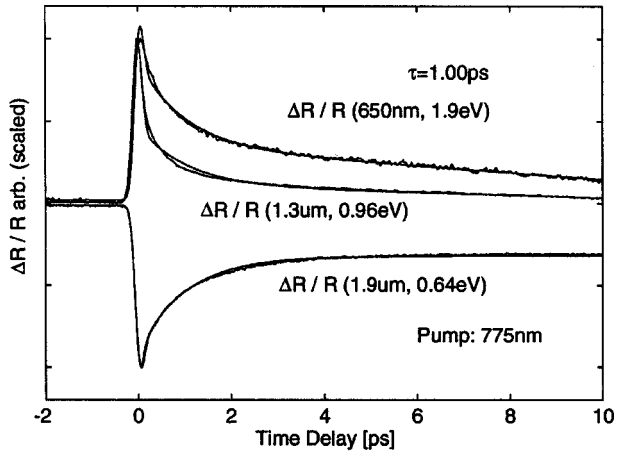

FIG. 2. Pump-probe time-resolved differential reflectance obtained for Rb_3C_{60} at room temperature for a pump excitation at 775 nm (1.60 eV) and various probe wavelengths smaller than and greater than that of the pump.

The experimental $\Delta R(t)/R$ traces in Figs. 1 and 2 were fitted to a response function described by the cross correlation of pump and probe $g(t)$, and to a sum of three components: a δ function, an exponential decay with a decay time τ, and a step function c matched to the residual level:

$$\Delta R(t)/R = \int_{-\infty}^{\infty} d\xi\, g(t-\xi)[a\,\delta(\xi) + b\,\exp(-\xi/\tau) + c]. \tag{1}$$

The function $g(t)$ peaks at $t=0$, and dies off rapidly for $|t|>0$, with a width of ≈ 200 fs. The temporal responses for the two samples after the large initial change $\Delta R(0)/R$ show only small changes with probe wavelength. A fixed, wavelength-independent decay time of τ was thus used in fitting the data. This time constant was chosen to be the same as the τ's obtained from the 20 fs Ti:sapphire data:[44] $\tau = 0.7$ ps for K_3C_{60} (Fig. 1) and $\tau = 1.0$ ps for Rb_3C_{60} (Fig. 2). Only the relative contributions of the different components (a,b,c) were optimized for each trace individually. The resulting least squares fits are shown with the data. A good fit is obtained in all cases except for some small deviation in the 1.3 μm probe arrangement for the rubidium-doped film (see Fig. 2).

The most striking feature in the wavelength-dependent data (see Figs. 1 and 2) is the sign change of the pump-probe response between 650 nm and 1.3 μm for K_3C_{60}, and between 1.3 and 1.9 μm for Rb_3C_{60}. For Rb_3C_{60}, this sign change is observed for both the reflection and transmission data. Transmission could not be observed in K_3C_{60}, since the samples were too thick. As we will see in Sec. V, the sign changes can be interpreted as due to a combination of factors, including whether the interband transition produced by the probe frequency originates from above or below the Fermi level.

IV. CARRIER DYNAMICS IN THE SUPERCONDUCTING PHASE

A. Optics

We used a 775 nm (1.6 eV) pump and 2 μm (0.64 eV) probe setup for our low-temperature measurements because we expected the sensitivity to changes in the quasiparticle dynamics occurring around the Fermi level to be larger for lower-energy photons. Unfortunately, 0.64 eV is still much larger than the superconducting gap $2\Delta \approx 3.5 k_B T_c$, which is about 8.5 meV for Rb_3C_{60} and 5.5 meV for K_3C_{60}. However, at room temperature a considerably larger signal is obtained for a 2 μm probe compared to both a 1.3 μm and a 775 nm probe, thus allowing us to perform the experiment at lower excitation intensity levels. It is very important to keep the laser fluence low to reduce thermal heating and to keep the increase in the transient electron temperature lower than the superconducting transition temperature. If the transient increase in electron temperature is too high, say 300 K–1000 K as reported for many room-temperature pump-probe experiments (see, for example, Ref. 45), the response will be

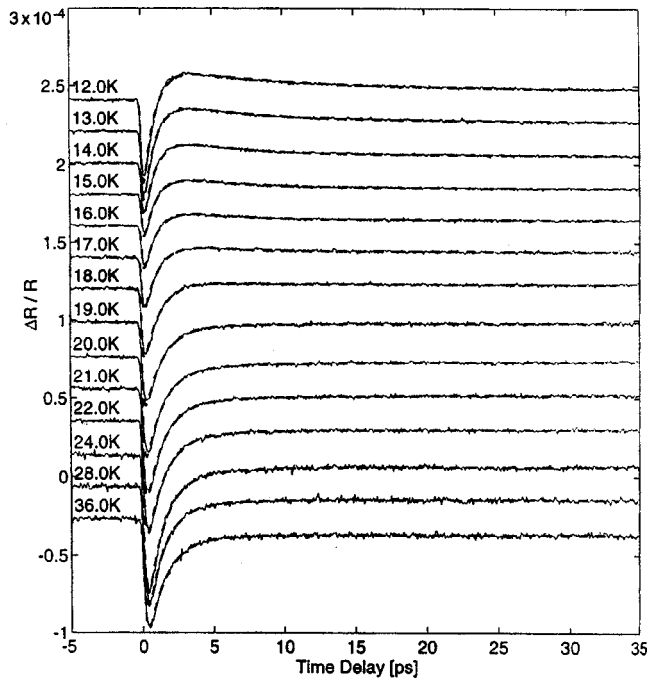

FIG. 3. Ultrafast optical $\Delta R(t)/R$ response in K_3C_{60} at a series of nominal temperatures above and below the superconducting phase transition of $T_c = 18$ K. Pump and probe wavelengths of 775 nm and 2 μm, respectively, were used for the $\Delta R(t)/R$ measurements. The fitting of the $\Delta R(t)/R$ results to Eq. (2) using temperature-dependent parameters (see discussion in text) is given by the dashed curves.

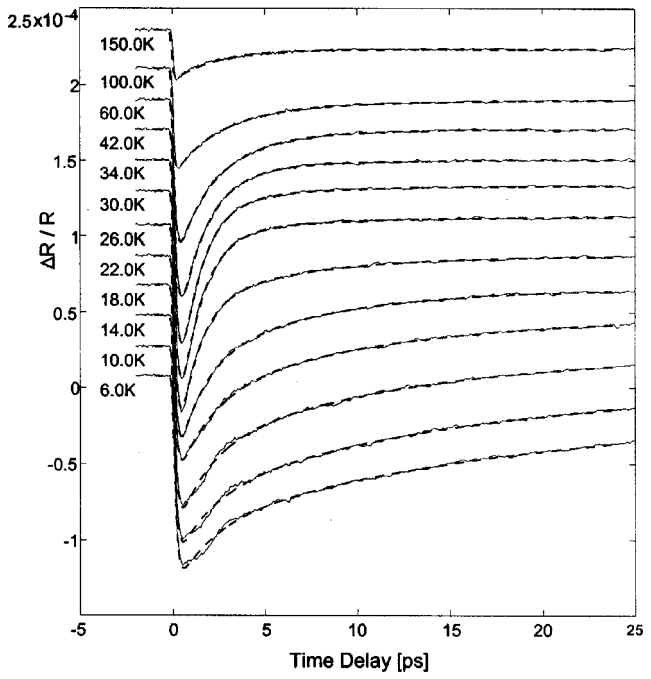

FIG. 4. Change in reflectivity $\Delta R(t)/R$ versus pump-probe delay time for Rb_3C_{60} at a series of sample temperatures above and below the superconducting phase transition of $T_c = 28$ K. Pump and probe wavelengths of 775 nm and 2 μm, respectively, were used for the $\Delta R(t)/R$ measurements. The fitting of the $\Delta R(t)/R$ results to Eq. (2) using temperature-dependent parameters (see discussion in text) is given by the dashed curves.

dominated by the initial thermalization, which monitors Fermi level smearing and is not related to Cooper pair recombination or other quasiparticle processes related to superconductivity. Unfortunately, the electronic specific heat capacity in the normal state is proportional to temperature, causing a ten times larger increase in the induced electronic heating at 30 K as compared to room temperature. This heating effect is, however, compensated by an increase in signal size, which partially makes up for this disadvantage.

To monitor the quasiparticle dynamics at such low temperatures, a high-repetition-rate (83 MHz) source is absolutely essential to keep the excitation intensity low and to achieve a good signal detectability. The pump was obtained straight from the Ti:sapphire laser oscillator operating at 775 nm, and the 2 μm idler from a synchronously pumped optical parametric oscillator served as the probe.[8] For this wavelength combination, we have a time resolution of 200 fs or better, given by the full width at half maximum of the cross correlation between pump and probe. Both pump and probe were focused to a ≈ 100 μm spot with an average power of about 0.7 mW (80 nJ cm^{-1}) for the pump and 0.6 mW (70 nJ cm^{-1}) for the low-intensity probe incident on the film. The pump was double chopped at 6 MHz and at 2 kHz to improve the signal detectability and to discriminate against rf pickup. The M_3C_{60} films have a low reflectivity, and after reflection by the film the collected and detected probe light amounted to only about 5 μW.

Shot-noise-limited detection at this wavelength, using such low power levels, and using MHz modulation frequencies, was quite challenging. The probe signal modulation was monitored with a 100 μm diameter, 100 MHz bandwidth, 2.4 μm extended wavelength sensitivity strained-layer InGaAs photodiode. A tuned preamplifier with the photodiode an integral part of the resonant tank circuit, buffered by a field-effect transistor–bipolar cascade circuit, was used to obtain shot-noise-limited $\Delta R(t)/R$ sensitivity down to only a few microwatts of detected power at our probe wavelength of 2 μm and at our modulation frequency of 6 MHz.[8]

B. Pump-probe data through the superconducting phase transition

In Fig. 3 we plot the change of the reflectivity $\Delta R(t)/R$ for K_3C_{60} at a series of nominal temperatures above and below the superconducting phase transition of $T_c = 18$ K. The curves are not corrected for the average heating of the lattice by the laser, which is estimated to be on the order of 1 K. A similar plot for the induced reflection change $\Delta R(t)/R$ for Rb_3C_{60} is shown in Fig. 4. Both samples show a three- to fivefold increase in the signal size when the samples are cooled down from room temperature to about 100 K, which is consistent with the decreased electronic specific heat.[36] At room temperature the signals are characterized by a $\Delta R(t)/R$ transient that decays within ≈ 0.7 ps for K_3C_{60} and ≈ 1.0 ps for Rb_3C_{60}. The normal state decay time increases by about a factor of 2 for both samples as the temperature is lowered from room temperature to about 50 K. This response is typical for metallic systems in which nonequilibrium carriers are cooled via inelastic collisions with phonons.[11]

In order to analyze the $\Delta R(t)/R$ results in more detail, the pump-probe data were fitted with a combination of re-

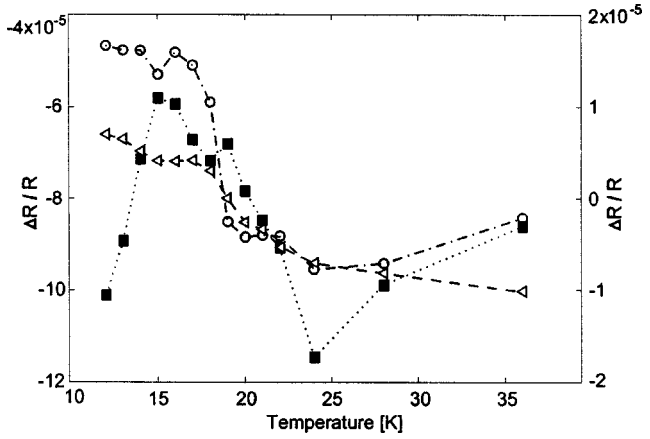

FIG. 5. Temperature dependence of the linear fitting parameters b_1 (dotted curve, squares), b_2 (dot-dashed curve, circles), and c (dashed curve, triangles) to Eq. (2) for the experimental $\Delta R(t)/R$ data for K_3C_{60}. The left hand scale refers to b_1, while the right hand scale refers to b_2 and c. The lines are a guide to the eye.

sponses: (i) a fast exponential decay time (τ_1) on the order of 1 ps to represent the fast exponential decay associated with the thermal relaxation of the excited electrons via collisions with phonons (this response is observed in both the normal and superconducting phases); (ii) a second slower exponential decay time (τ_2) to account for the slow decay present only below T_c; (iii) a step function (c) matched to the residual level to account for long-lived responses ($\tau > 100$ ps); (iv) a rise time (τ_R) to model the considerably slower response to the pump around the transition temperature. The δ-function term [see Eq. (1)] observed at room temperature was found to be negligible at low temperatures.

This analysis results in a fitting equation with three time constants and a few linear coefficients to match the contributions of the different exponential decays with the observed changes in $\Delta R(t)/R$. The calculated response was convolved with the measured cross-correlation function $g(t)$:

$$\Delta R(t)/R = \int_{-\infty}^{\infty} d\xi\, g(t-\xi)[1-\exp(-\xi/\tau_R)] \times [b_1 \exp(-\xi/\tau_1) + b_2 \exp(-\xi/\tau_2) + c]. \quad (2)$$

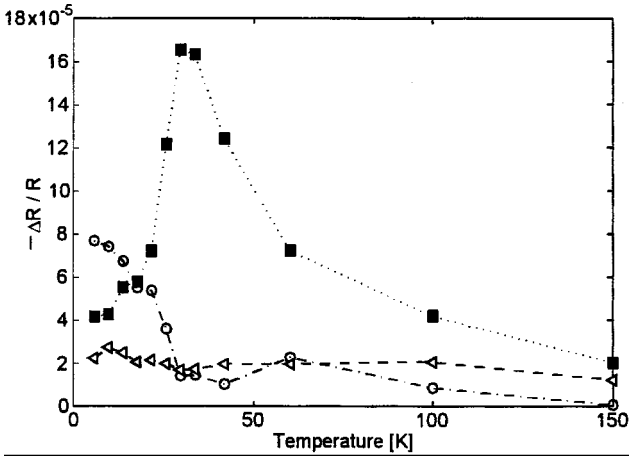

FIG. 6. Temperature dependence of the linear fitting parameters b_1 (dotted curve, squares), b_2 (dot-dashed curve, circles), and c (dashed curve, triangles) for the experimental $\Delta R(t)/R$ data for Rb_3C_{60}. The lines are a guide to the eye.

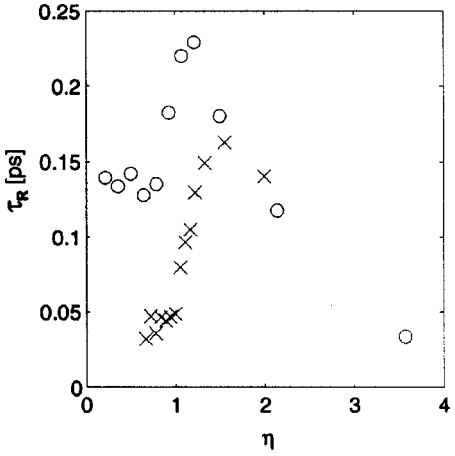

FIG. 7. Fitted rise times τ_R vs reduced temperature $\eta = T/T_c$ for K_3C_{60} (crosses) and Rb_3C_{60} (circles).

A full nonlinear least squares minimization over the three-dimensional τ-parameter time constant space (τ_R, τ_1, τ_2) was performed for each temperature. The parameters b_1, b_2, and c are linear fitting parameters to the experimental $\Delta R(t)/R$ data and can be calculated explicitly (Gauss-Newton least squares fitting) for each triplet set of time constants (τ_R, τ_1, τ_2).

The linear fitting parameters b_1, b_2, and c (in units of $\Delta R/R$) for K_3C_{60} and Rb_3C_{60} as a function of temperature are shown, respectively, in Figs. 5 and 6. The rise times τ_R, fast decay times τ_1, and slow decay times τ_2 for both K_3C_{60} and Rb_3C_{60} as a function of temperature are shown in Figs. 7, 8, and 9, respectively.

The resulting least squares fits to the data as a function of temperature are shown as dashed curves in Fig. 3 for K_3C_{60} and in Fig. 4 for Rb_3C_{60}. Good fits are obtained for all temperatures for both samples.

The slow exponential decay times (τ_2) characteristic for K_3C_{60} and Rb_3C_{60} in the superconducting phase, plotted in Fig. 9, decrease considerably as the temperature approaches the superconducting phase transition T_c from below. At the same time the amplitude of the slow response b_2 becomes diminishingly small and essentially disappears in the normal state (Figs. 5 and 6). This behavior is observed for both the

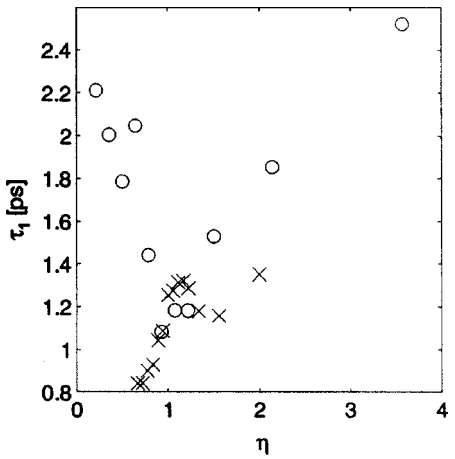

FIG. 8. Fast decay times τ_1 vs reduced temperature $\eta = T/T_c$ for K_3C_{60} (crosses) and Rb_3C_{60} (circles).

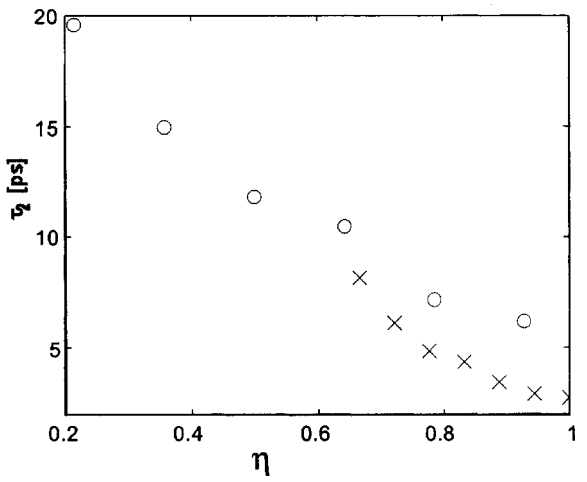

FIG. 9. Slow exponential decay time τ_2 as a function of reduced temperature $\eta = T/T_c$ for K_3C_{60} (crosses) and Rb_3C_{60} (circles).

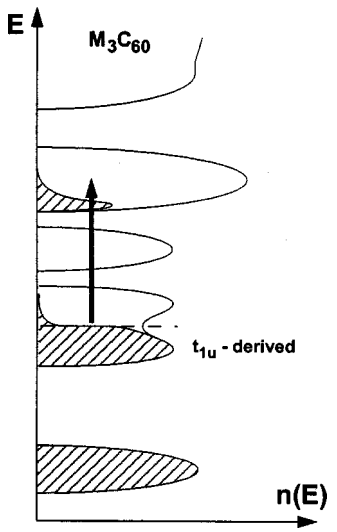

FIG. 10. Schematic plot of energy vs density of states for M_3C_{60} (M=K,Rb) where the oblique lines indicate occupied states (see discussion in Sec. III B).

Rb_3C_{60} and K_3C_{60} samples. The trend observed for the slow relaxation time τ_2 in both K_3C_{60} and Rb_3C_{60} (Fig. 9) is opposite to that predicted by the BCS theory.[46,47] This discrepancy points to the presence of an additional, dominant, slow decay mechanism for electronic excitation in K_3C_{60} and Rb_3C_{60}. Data we have taken on τ_2 in YBCO are similar to those obtained for YBCO by other researchers,[11–31] and appear to agree, at least approximately, with the BCS theory. Our YBCO results and comparison with the observations in K_3C_{60} and Rb_3C_{60} will be presented elsewhere.[8,38]

The most striking feature in the response of the K_3C_{60} data is the dip of about 30% in the absolute value of the fast component b_1 (Fig. 5). This reduction in signal size of the b_1 term is most pronounced in the vicinity of the transition temperature, and is discussed in Sec. V. Below T_c an additional slower component b_2 with *opposite sign* is observed, and this fitting parameter b_2 is negligibly small in the normal state. The amplitude of b_2 increases and the related decay time τ_2 becomes longer as the temperature is lowered below T_c. This effect is seen in Fig. 9 most clearly for Rb_3C_{60}, where the experimental data cover a larger temperature range below T_c.

The response of Rb_3C_{60} (Fig. 6) shows both differences from and similarities to the K_3C_{60} results in Fig. 5. The Rb_3C_{60} film also shows a slow component b_2 below the transition temperature T_c, and b_2 also becomes more pronounced as the temperature is lowered further. In the case of Rb_3C_{60}, the slower component b_2 has the *same sign* as the fast component b_1. Both K_3C_{60} and Rb_3C_{60} also exhibit a decrease in rise time τ_R (Fig. 7) and an increase in τ_2 (Fig. 9) as T drops below T_c. A model used to discuss these observations is presented in Sec. V.

V. ANALYSIS OF THE RESULTS

A. Model for analysis of the data

In contrast to C_{60}, the doped K_3C_{60} and Rb_3C_{60} films are metallic, and a simple band picture appears to provide a valid framework within which to interpret their pump-probe responses. As indicated in the schematic energy diagram for the doped samples given in Fig. 10, the half-filled t_{1u} orbital (odd parity) for isolated C_{60}^{3-} ions forms the conduction band for M_3C_{60}, and the only parity-allowed (and thus dominant) transitions at 2 eV are from the partially occupied t_{1u} band to some higher-lying band with even parity (such as h_g)[36] as indicated in Fig. 10. Subsequent to the optical excitation due to the pump, the energy delivered to the conduction band by the introduction of holes is redistributed rapidly by means of Coulomb scattering, raising the electron temperature. The electron gas then returns to the lattice temperature on a longer time scale via electron-phonon coupling.

We will then analyze our pump-probe $\Delta R(t)/R$ results on the basis of the following picture: The pump pulse delivers energy per unit volume ΔE to the sample near its surface by introducing holes relatively deep in the conduction band by interband transitions (see Fig. 10). The energy is quickly taken up by the conduction electrons, since the lattice cannot respond on the femtosecond time scale of the pump pulse. The electron distribution is raised to a slightly elevated temperature T_E, determined by the electronic specific heat, in a time on the order of a few femtoseconds. The change in electron temperature modifies the dielectric properties of the sample, which results in an initial change $\Delta R(0)/R$ in the reflectivity at the probe frequency. As the excess energy is gradually transferred to the lattice through the electron-phonon coupling, $\Delta R(t)/R$ returns to nearly zero in a decay time τ_1 of the order of picoseconds. The return of carriers from higher bands occurs after a longer time and does not play a significant role in the analysis of the experiments on a picosecond time scale.

When the sample becomes superconducting, the scenario changes somewhat. The energy ΔE delivered to the samples through the electronic excitation changes little, since the optical properties of K_3C_{60} and Rb_3C_{60} are essentially unchanged at the pump and probe optical frequencies. However, as the electron temperature returns toward its original value, the recombination of electron quasiparticles to form Cooper pairs acts as a bottleneck, contributing a slow component to the decay of $\Delta R(t)/R$, which is characterized by a decay time τ_2.

As we show, the best argument for this scenario in K_3C_{60} and Rb_3C_{60} is that it leads to a reasonable explanation of our pump-probe data in these materials. On the basis of this picture, we can identify the fitting parameters in Eq. (2). The parameters b_1 and b_2 are, respectively, the fast and slow decay contributions to $\Delta R(t)/R$; while τ_1 and τ_2 are, respectively, the times characterizing electron-phonon cooling and Cooper pair recombination. The small rise time fitting parameter τ_R represents a delay in the electron quasiparticle excitation due to Cooper pair bond breaking, or the delay time before the slow component due to the Cooper pairing bottleneck sets in.

B. Dielectric function

To understand the behavior of $\Delta R(t)/R$ for K_3C_{60} and Rb_3C_{60} with temperature, frequency, and time, we make use of an approximate complex dielectric function of the form previously used by Iwasa *et al.*[48] to give an excellent description of the reflectivity of K_3C_{60} at room temperature over a frequency range from ~ 0.2 eV to ~ 2 eV. The dielectric function used by Iwasa *et al.*[48] is

$$\epsilon(\omega)=\epsilon_\infty-\frac{\omega_p^2}{\omega(\omega+i\gamma_p)}+\frac{f_L\omega_L^2}{[(\omega_L^2-\omega^2)-i\gamma_L\omega]}. \qquad (3)$$

In Eq. (3), ϵ_∞ is the high-frequency limiting dielectric constant, ω_p is the conduction electron plasma frequency, γ_p is the effective electron intraband relaxation rate, and ω is the frequency of the light beam incident on the sample surface. Here ω_L and γ_L are the effective resonant frequency and damping rate, respectively, representing interband transitions between the partially filled conduction band and higher-lying empty bands in K_3C_{60}; and f_L represents a dimensionless measure of the rate of interband transitions. The values of the room temperature parameters that Iwasa *et al.* found to give the best fit[48] of their reflectivity vs frequency data in K_3C_{60} are $\epsilon_\infty=5.44$, $\omega_p=1.56$ eV, $\gamma_p=0.308$ eV, $f_L=0.826$, $\omega_L=1.05$ eV, and $\gamma_L=0.563$ eV. The incident light frequency ω in Eq. (3) is also in eV.

Although Eq. (3) was applied in Ref. 48 only to K_3C_{60}, the reflectivity spectra of Rb_3C_{60} and K_3C_{60} are quite similar,[49] so we expect the form of Eq. (3) to apply approximately to both materials, but with somewhat different values for the parameters for Rb_3C_{60}. However, we note that Eq. (3) can also be viewed as a parametrized expression for the dielectric function, guided by a physical model, which gives a good fit to the reflectivity data over a range of frequencies with a minimal set of fitting parameters. But, for a given frequency, the reflectivity does not uniquely determine the parameters. We will find, in applying Eq. (3) to our experimental results obtained with the probe pulse at 0.64 eV, that the parameters used by Iwasa *et al.*[48] must be modified slightly to give the best explanation of our $\Delta R(t)/R$ results, while changing the fit to the $R(\omega)$ reflectivity data minimally.

We will first apply Eq. (3) to K_3C_{60}, initially using Iwasa's room-temperature parameters. These parameters are then modified slightly to apply to the $\Delta R(t)/R$ data for K_3C_{60} at low temperatures. We discuss further below the changes required to explain the observations in Rb_3C_{60}.

C. The calculation of $\Delta R(t)/R$

We make the assumption that, after the arrival of the pump pulse, the change in reflectivity at the probe frequency is predominantly due to changes in the population and density of states at the points in the conduction band corresponding to $\vec{k}$-conserving transitions at the probe frequency. It should be noted that the set of $\vec{k}$-conserving transitions over the conduction band may not correspond to a single fixed initial state energy relative to the Fermi level. We will assume that these transition points are dominated by those at an energy E relative to the Fermi level, which could correspond to a maximum in the joint density of states. We will refer to the corresponding set of $\vec{k}$ states in the conduction band as the ''initial points.''

This model implies that the change in reflectivity produced by the pump pulse is mainly due to changes in the oscillator strength f_L of Eq. (3). Based on Eq. (3) and the physical model we have outlined, we therefore write the expression for $\Delta R(t)/R$ for small changes in electron temperature in the form

$$\frac{\Delta R(t)}{R}=\frac{1}{R}\frac{\partial R}{\partial \epsilon}\frac{\partial \epsilon}{\partial f_L}\Delta f_L(t)=Q\Delta f_L(t), \qquad (4)$$

where

$$Q=2\,\mathrm{Re}\left(\frac{\partial\epsilon/\partial f_L}{\sqrt{\epsilon}(\epsilon-1)}\right). \qquad (5)$$

To obtain Eq. (5) from Eq. (4), we have used the well known normal incidence formula,

$$R=\left|\frac{\sqrt{\epsilon}-1}{\sqrt{\epsilon}+1}\right|^2. \qquad (6)$$

To describe the initial $t=0$ change in $\Delta R(0)/R$, we assume that a small change in temperature ΔT is produced by the pump, yielding

$$\Delta R(0)/R=Q\Delta f_L(0), \qquad (7)$$

where

$$\Delta f_L(0)=\frac{\partial f_L}{\partial T}\frac{\Delta E}{C_e(T)}=\frac{\partial f_L}{\partial \eta}\frac{1}{C_e'(\eta)}\frac{\Delta E}{(\gamma T_c^2)}. \qquad (8)$$

In Eq. (8), ΔE is the energy per unit volume delivered to the conduction electrons by the pump and $C_e(T)$ is the electronic specific heat. We have introduced the normalized (reduced) temperature $\eta=T/T_c$ and the normalized electronic specific heat $C_e'(\eta)=C_e(T)/\gamma T_c$, where γT is the temperature dependence of $C_e(T)$ above T_c. Based on the fitting parametrization of the data in Eq. (2), we identify Eq. (7) with the sum of b_1+b_2. For convenience in the later discussion, we define

$$\Delta f_L(0)=\frac{\Delta E}{(\gamma T_c^2)}\sigma(0), \qquad (9)$$

where

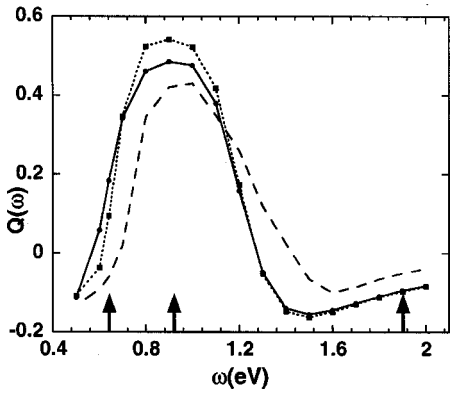

FIG. 11. Plot of Q vs ω for K_3C_{60} and Rb_3C_{60} where Q is defined by Eq. (5). The squares (dotted curve) represent calculations using parameters of Ref. 48 for K_3C_{60} at room temperature, $\omega_p=1.56$ eV and $\gamma_p=0.308$. The circles (solid curve) represent a set of parameters for K_3C_{60} in which $\omega_p=1.52$ eV and $\gamma_p=0.380$ eV at room temperature (see text in Sec. V E). The dashed curve represents a qualitative sketch of a possible picture of $Q(\omega)$ vs ω for Rb_3C_{60} that is based on a modified set of parameters in Eq. (5) and is consistent with the experimental results shown in Figs. 2 and 6 (see text in Sec. V E). The arrows indicate the probe frequencies used in the room-temperature experiments.

$$\sigma(0)=\frac{\partial f_L}{\partial \eta}\frac{1}{C_e'(\eta)} \tag{10}$$

and $\eta=T/T_c$.

D. Room-temperature data

We have analyzed first the room-temperature results for $\Delta R(0)/R$ in K_3C_{60} using Eqs. (5) and (7). The quantity Q in Eq. (5) was first evaluated as a function of ω using the room-temperature parameters of Iwasa *et al.* in Eq. (3). The results for $Q(\omega)$ vs ω are plotted in Fig. 11, and indicate that Q changes sign at $\omega\sim1.25$ eV. If all three room-temperature probe spectra in K_3C_{60} shown in Fig. 1 (at frequencies of 0.64 eV, 0.96 eV, and 1.92 eV) originate from initial points in the conduction band below the Fermi level, then clearly $\Delta f_L(0)$ is negative, since $df_L/d\eta$ is negative below the Fermi level. The results for $\Delta R(0)/R$ shown in Fig. 1 for K_3C_{60} are then consistent with the frequency dependence of Q in Fig. 11, both as to sign and to the frequency for the sign reversal. The only possible discrepancy between the data (solid curve) and the experimental results in Fig. 1 is the prediction that Q is considerably larger for 0.96 eV than for 0.64 eV, while the reverse is true for the experimental data for $\Delta R(t)/R$ shown in Fig. 1. This disparity will be discussed in Sec. V E. In Fig. 11 we also show a plot of Q vs ω for K_3C_{60} with a set of parameters slightly different from those of Iwasa *et al.*[48] The reason for considering this alternate set of parameters will be discussed in Sec. V E.

The data in Fig. 2 for Rb_3C_{60} are similar to those for K_3C_{60}, but the sign reversal occurs at a frequency below 0.96 eV, indicating that Eq. (3) with the parameters of Iwasa's *et al.* for K_3C_{60} does not give an accurate description of the experimental pump-probe data for Rb_3C_{60}, as might be expected. We also show in Fig. 11 a sketch of a possible curve of $Q(\omega)$ vs ω consistent with the $\Delta R(t)/R$ results for Rb_3C_{60} (see Sec. V E).

E. Low-temperature results

The complex dielectric function $\epsilon(\omega)$ of the form given in Eq. (3) gives a good description of R vs ω and the sign of Q vs ω observed in K_3C_{60} at room temperature. The term in Eq. (3) proportional to f_L represents the contribution of interband transitions to the dielectric function, and the resonant denominator provides an empirical description of the dependence of $\epsilon(\omega)$ on frequency for the value of the conduction band density of states and population at the transition points associated with that frequency. If the band gaps and other band parameters in a material do not depend strongly on temperature, then changes in the interband contribution to the dielectric function as the temperature is lowered from room temperature can be described by the appropriate changes in f_L with temperature.

To apply Eq. (3) to our *low-temperature* data, we will then make the reasonable assumption that only f_L and γ_p must be modified. The former must change because the interband transition rate is a function of the density of states (which changes in the superconducting state) and of the population of electrons $f(E)$ at the transition points; and the latter must change because the intraband scattering rate changes with temperature. As we shall show, our results can be fitted reasonably well as a function of temperature if the interband transition at the pump frequency (1.6 eV) originates at an energy E well below the Fermi level for both K_3C_{60} and Rb_3C_{60}; and the corresponding energies for K_3C_{60} and Rb_3C_{60} at the probe frequency (0.64 eV) are, respectively, $E\sim0.0075$ eV below and $E\sim0.0086$ eV above the Fermi level.

The electrical resistivities of K_3C_{60} and Rb_3C_{60} versus temperature are quite similar and are nearly independent of temperature from about 100 K down to their respective transition temperatures of 18 K and 28 K. Depending on the method of sample preparation, the resistivities of these materials drop by a factor of from 2 to 5 from room temperature down to 100 K. We take this factor for our samples as roughly 2, and using this factor to scale the value of Iwasa's *et al.* for γ_p, we arrive at an approximate low-temperature value of $\gamma_p=0.154$ eV for K_3C_{60} from 100 K down to its superconducting transition temperature, and also below T_c. For simplicity, we have used the same low-temperature value of $\gamma_p=0.154$ eV for Rb_3C_{60}.

To evaluate the temperature dependence of $\Delta R(0)/R$ predicted by Eqs. (7) and (8), we must consider the dependence of both Q and $\Delta f_L(0)$ on temperature as T is lowered. We consider first the case for $\eta=T/T_c>1$. As discussed above, we scale f_L for $\eta>1$ as

$$f_L=0.826\frac{(e^{u/\eta_R}+1)}{(e^{u/\eta}+1)}, \tag{11}$$

where we have introduced the normalized energy at the transition points E relative to the Fermi level $u=E/(kT_c)$; and η_R is η at room temperature. When u in Eq. (11) is negative we are dealing with interband transitions from below the

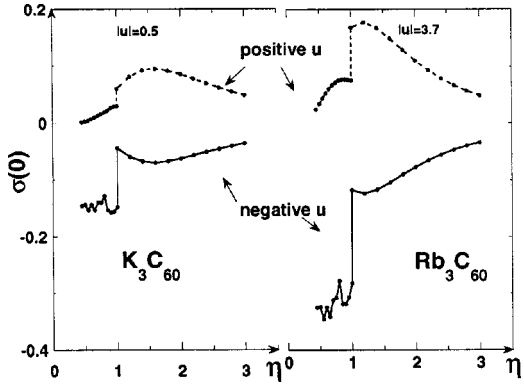

FIG. 12. Plots of $\sigma(0)$ vs η for the values of $|u|$ that best fit the $\Delta R(0)/R$ data for K_3C_{60} and Rb_3C_{60} with $\eta>1$. Here $\sigma(0)$ is defined by Eq. (10), η is the reduced temperature $\eta=T/T_c$, and $u=E/kT_c$. The upper curves correspond to positive u and the lower curves to negative u. Comparison of the results for $\eta>1$ and $\eta<1$ with experiment allows us to establish appropriate values as $u=-5.0$ (K_3C_{60}) and $u=+3.7$ (Rb_3C_{60}) (see text in Sec. V E).

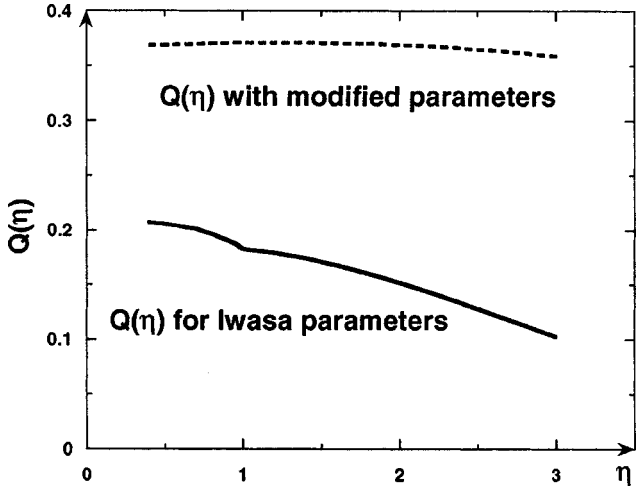

FIG. 13. Plot of Q vs η for K_3C_{60} for the low-temperature parameters of Ref. 48 ($\omega_p=1.56$ eV and $\gamma_p=0.154$) shown in the solid curve, and for modified low-temperature parameters ($\omega_p=1.52$ eV and $\gamma_p=0.190$) shown in the dashed curve (see text in Sec. V E). Here Q is defined by Eq. (5) and η is the reduced temperature $\eta=T/T_c$.

Fermi level, while a positive value of u implies transitions from above the Fermi level. As we will show, a fairly good explanation of the data for both $\eta>1$ and $\eta<1$ can be obtained with $u=-5.0$ for K_3C_{60} and $u=+3.7$ for Rb_3C_{60}.

Figure 12 shows a plot of $\sigma(0)$ as a function of η for values of u that best mirror the behavior of $\Delta R(0)/R$ for $\eta>1$ in K_3C_{60} and Rb_3C_{60}. In view of the overall similarity between the K_3C_{60} calculation for $\sigma(0)$ and the b_1 data of Fig. 5, it is reasonable to assume that the observed point in $\Delta R(t)/R$ at 24 K is due to some accidental experimental fluctuation. The shapes of the calculated curves for positive and negative u in Fig. 12 are identical (except for a change in sign) for $\eta>1$, but the amplitudes are different because the scaling factor $(e^{u/\eta_R}+1)$ in Eq. (11) depends on the sign of u.

Whether the curve of $\sigma(0)$ for positive or negative values of u corresponds to the observed spectrum depends on the sign of Q [see Eq. (5)]. However, while the shape of the spectrum for K_3C_{60} in Fig. 12 gives a good description of the temperature dependence of the data in Fig. 5 for $\eta=T/T_c>1$, the plot of Q vs η for K_3C_{60}, shown in Fig. 13 with the parameters of Iwasa *et al.*, indicates a strong temperature dependence for $\eta>1$, spoiling the apparent agreement. The origin of the strong temperature dependence of Q is the appearance of the factor $(\epsilon-1)$ in the denominator of the expression for Q given in Eq. (5). With the parameters of Iwasa *et al.*, the real part of $\epsilon(\omega)$ is only slightly greater than 1 for $\omega=0.64$ eV, causing a great sensitivity of Q to temperature.

One approach to resolving this problem is to accept the predicted variation of Q with temperature and to modify $\sigma(0)$ in Eq. (10) so that the product $Q\sigma(0)$ predicts the observed temperature dependence of $\Delta R(0)/R$. Another approach is to note that a small change in the parameters ω_p and γ_p can increase the value of the real part of ϵ to the point where Q varies only slightly with temperature. This can occur with no change in the calculated value of R at $\omega=0.64$ eV, and only slight changes in R at other neighboring frequencies. As an example, we have examined the effect of changing the room-temperature parameters of Iwasa *et al.*, ω_p and γ_p, from 1.56 to 1.52 eV, and 0.308 to 0.380 eV, respectively. This produces a change in the room-temperature reflectivity at the probe frequency 0.64 eV of less than 0.1%, while not changing $\sigma(0)$ at all. For the low-temperature calculation ($T<100$ K), the low-temperature parameters of Iwasa *et al.* ($\gamma_p=0.154$, $\omega_p=1.56$ eV) change in the modified calculation to the low-temperature parameters ($\gamma_p=0.190$, $\omega_p=1.52$ eV). The effect of these parameter changes on the Q vs η plot is shown in Fig. 13, where Q for the modified ω_p and γ_p is seen to change only slightly for all η. Thus, a reasonable explanation of the temperature dependence of $\Delta R(0)/R$ for $\eta>1$ can be obtained for K_3C_{60} from the plot of $\sigma(0)$ vs η shown in Fig. 12 for $|u|=5.0$.

The effect of these parameter changes on the $Q(\omega)$ vs ω plot at room temperature is shown by the solid curve through the filled circles in Fig. 11, where it is seen that the modified parameters lead to an increase in Q at $\omega=0.64$ eV relative to the dotted curve through the square points using the parameters of Iwasa *et al.* This result, along with a possible larger value of $\sigma(0)$ at 0.64 eV than at 0.96 eV, could help to explain the larger value of $\Delta R(0)/R$ observed for 0.64 eV at room temperature in Fig. 1.

For $\eta<1$, the effects due to the onset of superconductivity must be considered. There is good experimental evidence that both K_3C_{60} and Rb_3C_{60} are weak coupling BCS superconductors.[36] In BCS theory, a gap of 2Δ opens up at the Fermi level,[50,51] and the density of states for electron quasiparticles peaks up at the gap boundaries. The reduced specific heat increases abruptly below T_c, and for $\eta<1$ is given approximately in the BCS theory[51] by

$$C_e'(\eta)=9.17e^{-(1.5/\eta)}, \tag{12}$$

where $\eta=T/T_c$.

These abrupt changes below T_c are reflected in Eqs. (7) and (8), in particular by the modification of the temperature dependence of f_L, which, in the BCS theory, becomes

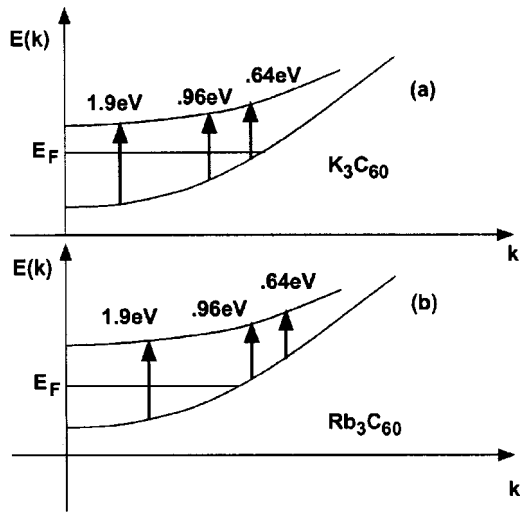

FIG. 14. Sketch of a possible model of the interband transitions relative to the Fermi level E_F at the three probe frequencies indicated. This placement of E_F leads to a consistency between the experimental data in Figs. 1 and 2 and our modeling of $\Delta R(t)/R$ for (a) K_3C_{60} and (b) Rb_3C_{60} (see text in Sec. V E).

$$f_L = 0.826 \frac{(e^{u/\eta_R}+1)}{(e^{u/\eta}+1)} \times \frac{|u|}{(u^2-\delta^2)^{1/2}}, \tag{13}$$

where $\delta = \Delta(T)/kT_c$ and $2\Delta(0)$ is the superconducting energy gap at $T=0$. The low-temperature limiting value of δ in the BCS theory is 1.75.[51] For $\eta<1$, the changes due to BCS effects have been included in the dielectric function, and have been included in the calculations of $Q(\eta)$ vs η (Fig. 13) and of $\sigma(0)$ vs η (Fig. 12). In performing these calculations, we have used approximate values of $\Delta(\eta)$ read from a graph obtained from BCS theory,[51] leading to some scatter in the calculated points. The striking difference in the behavior of $\sigma(0)$ in Fig. 13 between positive and negative values of u for $\eta<1$ should be noted. While the temperature-dependent peaking of the density of states below the Fermi level produces a large effect, the small values of f_L above the Fermi level prevent a similar result except when u approaches δ.

The results for K_3C_{60} shown in Fig. 12 for positive u are inconsistent with the experimental data of Fig. 5, and therefore imply that the interband transition at a probe frequency of 0.64 eV originates from conduction band states *below* the Fermi level. This conclusion is also consistent with the room-temperature frequency dependence of Q in Fig. 11, and suggests the qualitative picture of the three interband transitions in K_3C_{60} shown in Fig. 14.

The results for $\sigma(0)$ shown in Fig. 12 for Rb_3C_{60} for $\eta<1$ are inconsistent with negative u, and therefore indicate that the interband transitions originate from states *above* the Fermi level. A possible model for the three interband transitions of Fig. 2 for Rb_3C_{60} is also shown in Fig. 14. For this model to be consistent with the three room-temperature experimental spectra shown in Fig. 2, the frequency dependence of $Q(\omega)$ for Rb_3C_{60} must be somewhat different from that for K_3C_{60}. In Fig. 11 we sketch a possible qualitative picture of $Q(\omega)$ vs ω for Rb_3C_{60} which is consistent with the three observed $\Delta R(t)/R$ pump-probe spectra shown in Fig. 2.

There are sharp discontinuities appearing in the calculated spectra of Fig. 12 at the superconducting phase transition. These discontinuities are due to the abrupt change in the electron specific heat at $\eta=1$. In the actual experiment, neither the temperature of the sample nor its rise due to the pump pulse are uniform over the region of the probe pulse, so that a sharp discontinuity would not be expected in the experimental data. This argument can in part explain the differences in temperature dependence between the experimental results of Figs. 5 and 6 and our calculations in Fig. 12 in the vicinity of $\eta=1$.

VI. DISCUSSION

A. Fast relaxation time τ_1

For $T>T_c$, the low-temperature relaxation time τ_1 in the normal state should be well described by the theory due to Allen.[52] If the pump pulse produces an excited electron thermal distribution at an electron temperature T_E, then this distribution will relax toward the initial lattice temperature T_L by the emission of phonons. For a small rise in temperature ΔT, this process involves primarily acoustic phonons, assuming that the frequencies for the optical phonons ω_0 are greater than $kT/\hbar$. In this case, after the pump pulse the rate of energy loss per unit volume as given by Allen's theory is

$$\partial E/\partial t = C_e(T_E)\partial T/\partial t = -\pi\hbar n\rho(E_F)\lambda\langle\omega^2\rangle k(T_E - T_L). \tag{14}$$

Here n is the electron density, $\rho(E_F)$ is the electronic density of states at the Fermi level, and $\lambda\langle\omega^2\rangle$ is a measure of the coupling of electrons to the acoustic phonons of the material. Thus, we can write $\partial T/\partial t$ as

$$\partial T/\partial t = -\Delta T/\tau_1, \tag{15}$$

where

$$\tau_1 = \frac{C_e(T_E)}{\pi\hbar n\rho(E_F)\lambda\langle\omega^2\rangle k}. \tag{16}$$

For $T>T_c$, we have $C_e(T_E)=\gamma T_E$ where

$$\gamma = \pi^2 n\rho(E_F)k^2/3, \tag{17}$$

and

$$\tau_1 = \frac{\pi k T_E}{3\hbar\lambda\langle\omega^2\rangle}. \tag{18}$$

The excited electron temperature T_E is approximately equal to the initial lattice temperature T_L for small ΔT. The linear relationship between τ_1 and T_L is reasonably well satisfied for Rb_3C_{60} for $T>T_c$ in Fig. 8.

The linear relationship between τ_1 and T_E in low-temperature pump-probe experiments has been verified in a large number of materials, and the values of $\lambda\langle\omega^2\rangle$ obtained from Eq. (18) compare well with other experimental estimates of $\lambda\langle\omega^2\rangle$.[52,53] The quantities λ and $\langle\omega^2\rangle$ appear separately in an expression for T_c given by McMillan.[54] Pump-probe measurements in a number of materials combined with other data have been found to give reasonably good results for T_c obtained from the McMillan formula.[52,53] However,

$\lambda\langle\omega^2\rangle$ obtained from Eq. (18) and applied to our data for K_3C_{60} and Rb_3C_{60} yields much too low a value of T_c. This is not surprising, since our measurements of τ_1 determine $\lambda\langle\omega^2\rangle$ for acoustic phonon coupling, while superconductivity in K_3C_{60} and Rb_3C_{60} is believed to be due mainly to optical phonon coupling.[36]

For $T<T_c$, the data for τ_1 for K_3C_{60} were obtained over too limited a range in temperature to identify a trend for the T dependence of τ_1. However, for Rb_3C_{60}, τ_1 rises rapidly as T drops below T_c. A number of parameters affecting τ_1 in the superconducting state change, including electron quasiparticle coupling to acoustic phonons and the density of states near the energy gap. However, the main contribution to the sudden rise of τ_1 as T drops below T_c comes from the abrupt increase in electronic specific heat, as we can see from Eq. (16). Thus Allen's theory, with suitable modification of parameters in the superconducting state, may also explain τ_1 below T_c.

B. Slow relaxation amplitude b_2

To understand the slow relaxation amplitude b_2 in the superconducting state, we consider in more detail the model of the Cooper pair bottleneck introduced in Sec. V A. In the superconducting phase, the electron temperature T_E is raised by an amount ΔT above the lattice temperature T_L by the arrival of the pump pulse. The electron quasiparticle system begins to cool down rapidly at a rate determined by the fast relaxation time τ_1. At some point during this process, the Cooper pair bottleneck sets in, trapping excess quasiparticles above the superconducting gap. The quasiparticles continue to cool rapidly via interaction with acoustic phonons until a quasiequilibrium is reached, in which the distribution has returned to nearly the lattice temperature T_L, but with an excess of quasiparticles trapped above the gap, and a quasi Fermi level shifted down in energy because of missing population below the gap. Thereafter, the recombination of quasiparticles to form Cooper pairs continues at a rate determined by the slow relaxation time τ_2; while the entire distribution continues to cool toward the lattice temperature T_L, until true equilibrium is reached, with the disappearance of the excess population above the gap, and the return of the Fermi level to its original value.

With this picture in mind, we can qualitatively interpret the behavior of b_2 in K_3C_{60} and Rb_3C_{60}. Since $\Delta R(t)/R$ in Eq. (4) is proportional to $\Delta f_L(t)$, the contribution of the slow decay process to $\Delta R(t)/R$ is proportional to the change $\Delta f_{L_2}(t)$ produced by the bottleneck at the initial points of the interband transitions.

For initial points above the Fermi level (and not in the energy gap), the dominant contribution to $\Delta f_{L_2}(t)$ is due to the presence of excess quasiparticles, although there is a smaller contribution of opposite sign due to the upshift of u relative to the Fermi level (see Fig. 15). If the dominant contribution to $\Delta f_{L_2}(t)$ has the same sign as $\Delta f_L(0)$, then b_1 and b_2 must have the same sign. This is indeed the case for Rb_3C_{60} (see Fig. 6), consistent with our conclusion in Sec. V E that the initial points for the interband transitions in Rb_3C_{60} for a probe frequency of 0.64 eV lie above the Fermi level (see Fig. 14). Thus, as T falls below T_c, b_2 rises and ultimately saturates as the temperature drops well below T_c (see Fig. 6).

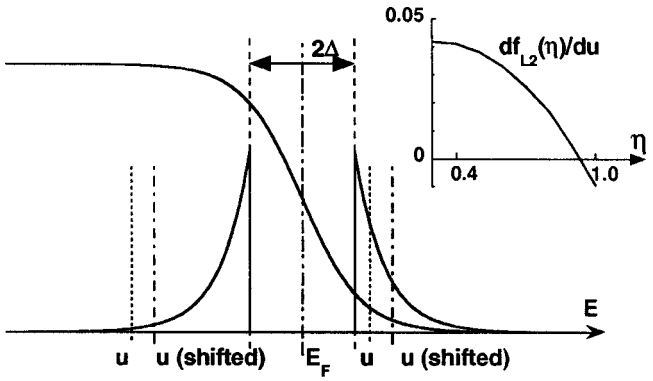

FIG. 15. Sketch of the Fermi level E_F, the positions of the gap edges, the excess BCS density of states, and the Fermi function before the arrival of the pump pulse. Examples of the initial transition points u above (positive) and below (negative) the Fermi level are shown by the dashed lines. Upon the arrival of the pump pulse, the electron system is raised in temperature. After a return to essentially the lattice temperature, trapping of excited carriers above the band gap shifts the quasi-Fermi level *down*, shifting the initial value of $u=E/kT_c$ *up* relative to the quasi-Fermi level, as shown by the dot-dashed lines. The inset shows the results of a calculation of df_{L_2}/du vs η for K_3C_{60} (see text in Sec. VI B).

For interband transitions with initial points below the Fermi level (see Fig. 14), the major contribution to $\Delta f_{L_2}(t)$ is caused by the downshift in the Fermi level due to the pump excitation, and the effective upshift of u associated with this downshift. The pump produces competing negative and positive contributions to $\Delta f_{L_2}(t)$ due, respectively, to changes in population and in the density of states (see Fig. 15). At the onset of the Cooper pair bottleneck, the value of b_2 is proportional to $\Delta f_{L_2}(0)=(df_{L_2}/du)\Delta u$, where f_{L_2} is given by Eq. (13), but with the normalization factor $[\exp(u/\eta_R)+1]$ held constant. A calculation of (df_{L_2}/du) for all values of u and reduced temperature η yields a positive value except for $\eta\sim 1$, implying that the sign of b_2 is opposite to that of b_1 for K_3C_{60} except near $\eta\sim 1$. A plot of (df_{L_2}/du) vs η for $u=-5.0$ (the value for K_3C_{60}) is shown as an inset in Fig. 15. The calculated result is quite similar to the observed curve of b_2 vs η for K_3C_{60} shown in Fig. 5, and, although the factor Δu determining $\Delta f_{L_2}(0)$ could also be temperature dependent, this result is consistent with our conclusion that the initial points for interband transitions in K_3C_{60} lie below the Fermi level.

VII. SUMMARY

Using femtosecond pump-probe techniques, we have studied the dynamics of electronic cooling in K_3C_{60} and Rb_3C_{60}. The change in reflectivity $\Delta R(t)/R$ was observed, both at room temperature and at low temperatures through the superconducting transition. The room-temperature data were taken at three different probe frequencies, while the low-temperature results were obtained at a single probe frequency. Both the room-temperature and low-temperature

data were well described by an empirical fit of $\Delta R(t)/R$, including a fast component due to electron cooling by phonon emission, and a slow component in the superconducting phase due to the recombination of Cooper pairs trapped above the gap during the cooling process.

The fast relaxation time τ_1 due to electron-acoustic phonon cooling, which could be followed over a broad range of temperatures only in Rb_3C_{60}, was found to have a linear dependence on lattice temperature above T_c, as expected from Allen's theory. τ_1 exhibited an abrupt rise by about a factor of 2 as the temperature dropped below T_c. The rise in τ_1 below T_c is mainly due to the sudden increase in electronic specific heat, as expected theoretically. This suggests that Allen's theory, with parameters suitably modified for superconductivity, may also describe energy loss to acoustic phonons below T_c.

The most striking finding of our experiments is the observation that, in both K_3C_{60} and Rb_3C_{60}, the temperature dependence of the Cooper pair recombination time τ_2 deviates drastically from the predictions of the BCS theory. There are many experiments that indicate that the M_3C_{60} compounds are BCS-like superconductors with Cooper pairing by means of optical phonons. The theoretical calculation of τ_2 in the BCS theory predicts a temperature dependence of the form $\tau_2 \propto \Delta(0)/\Delta(T)$, where $2\Delta(0)$ and $2\Delta(T)$ are the gaps at absolute zero and at temperature T, respectively. This form predicts that τ_2 becomes infinitely long at T_c, and drops to a flat finite value as temperature decreases below T_c. This prediction has been confirmed indirectly in quasiparticle tunneling experiments in the BCS superconductor tin, and a similar behavior has even been observed in pump-probe experiments on the high-temperature superconductor YBCO, which is known *not* to be a BCS-like superconductor. We have confirmed the behavior of τ_2 in YBCO with our own experiments; yet our observations in K_3C_{60} and Rb_3C_{60} indicate a finite value of τ_2 at T_c, followed by a monotonic *increase* in τ_2 as the temperature decreases below T_c. We will present a comparison of our results in YBCO with our K_3C_{60} and Rb_3C_{60} studies in a future publication.

ACKNOWLEDGMENTS

The work at MIT was supported by AFOSR through Agreement Nos. F49620-96-1-0160, F49620-95-1-0221, and F49620-96-1-0392, and by NSF Grant No. DMR-98-04734.

*Present address: Intel Corporation Research Laboratory, Santa Clara, CA.

†Present address: MathSoft, Inc., Cambridge, MA 02142-1521.

‡Present address: Jet Propulsion Laboratory, Pasadena, CA 911109.

§Present address: Department of Physics, University of Florida, Gainesville, FL 32611-8440.

[1] M. Lee, O. K. Song, J. C. Seo, D. Kim, Y. D. Su, S. M. Jin, and S. K. Kim, Chem. Phys. Lett. **196**, 325 (1992).

[2] T. W. Ebbesen, J. S. Tsai, K. Tanigaki, J. Tabuchi, Y. Shimakawa, Y. Kubo, I. Hirosawa, and J. Mizuki, Nature (London) **355**, 620 (1992).

[3] L. Degiorgi, G. Grüner, P. Wachter, S. M. Huang, J. Wiley, R. L. Whetten, R. B. Kaner, K. Holczer, and F. Diederich, Phys. Rev. B **46**, 11 250 (1992).

[4] A. F. Hebard, R. C. Haddon, R. M. Fleming, and A. R. Kortan, Appl. Phys. Lett. **59**, 2109 (1991).

[5] S. D. Brorson, M. K. Kelly, U. Wenschuh, R. Buhleier, and J. Kuhl, Phys. Rev. B **46**, 7329 (1992).

[6] G. P. Kochanski, A. F. Hebard, R. C. Haddon, and A. T. Fiory, Science **255**, 184 (1992).

[7] S. B. Fleischer, E. P. Ippen, G. Dresselhaus, M. S. Dresselhaus, A. M. Rao, P. Zhou, and P. C. Eklund, Appl. Phys. Lett. **62**, 3241 (1993).

[8] Siegfried Fleischer, Ph.D. thesis, Massachusetts Institute of Technology, 1997.

[9] I. Schuller and K. E. Gary, Phys. Rev. Lett. **36**, 429 (1976).

[10] I. Schuller and K. E. Gray, Solid State Commun. **23**, 337 (1977).

[11] G. L. Eesley, J. Heremans, M. S. Meyer, G. L. Doll, and S. H. Liou, Phys. Rev. Lett. **65**, 3445 (1990).

[12] W. Albrecht, T. Kruse, and H. Kurz, Phys. Rev. Lett. **69**, 1451 (1992).

[13] D. H. Reitze, A. M. Weiner, A. Inam, and S. Etemad, Phys. Rev. B **46**, 14 309 (1992).

[14] A. Frenkel, Phys. Rev. B **48**, 9717 (1993).

[15] S. G. Han, Z. V. Vardeny, K. S. Wong, O. G. Symko, and G. Koren, Phys. Rev. Lett. **65**, 2708 (1990).

[16] M. E. Gershenzon, V. V. Golovlev, I. B. Kedich, V. S. Letokhov, Yu. E. Lozovik, Yu. A. Matveets, E. G. Sil'kis, A. G. Stepanov, V. D. Titov, M. I. Falei, V. M. Farztdinov, S. V. Chekalin, and A. P. Yartsev, Pis'ma Zh. Éksp. Teor. Fiz. **52**, 1189 (1990) [JETP Lett. **52**, 602 (1990)].

[17] S. V. Chekalin, V. M. Farztdinov, V. V. Golovlyov, V. S. Letokhov, Y. E. Lozovik, Y. A. Matveets, and A. G. Stepanov, Phys. Rev. Lett. **67**, 3860 (1991).

[18] S. G. Han, Z. V. Vardeny, O. G. Symko, G. Koren, G. L. Eesley, J. Heremans, M. S. Meyer, and G. L. Doll, Phys. Rev. Lett. **67**, 1053 (1991).

[19] T. Gong, L. X. Zheng, W. Xiong, W. Kula, Y. Kostoulas, R. Sobolewski, and P. M. Fauchet, Phys. Rev. B **47**, 14 495 (1993).

[20] J. F. Young, T. Gong, P. J. Kelly, and P. M. Fauchet, Semicond. Sci. Technol. **9**, 465 (1994).

[21] R. Sobolewski, L. Shi, T. Gong, W. Xiong, X. Weng, Y. Kostoulas, and P. M. Fauchet, Proc. SPIE **2159**, 110 (1994).

[22] L. Shi, T. Gong, W. Xiong, X. Weng, Y. Kostoulas, R. Sobolewski, and P. M. Fauchet, Appl. Phys. Lett. **64**, 1150 (1994).

[23] A. L. Dobryakov, V. V. Golovlev, V. S. Letokhov, Yu. E. Lozovik, Yu. A. Matveets, A. G. Stepanov, V. M. Farztdinov, and S. V. Chekalin, Opt. Spectrosk. **76**, 975 (1994) [Opt. Spectrosc. **76**, 871 (1994)].

[24] Y. S. Lai, Y. Q. Liu, W. L. Cao, C. H. Lee, Zhi-Yuan Shen, P. Pang, D. J. Kountz, and W. L. Holstein, Appl. Phys. Lett. **66**, 1135 (1995).

[25] T. N. Thomas, C. J. Stevens, A. J. S. Choudhary, J. F. Ryan, B. Mihailovic, T. Mertelj, L. Forro, G. Wagner, and J. E. Evetts, Phys. Rev. B **53**, 12 436 (1996).

[26] J. Demsar, B. Podobnik, V. V. Kabanov, Th. Wolf, and D. Mihailovic, Phys. Rev. Lett. **82**, 4918 (1999).

[27] V. V. Kabanov, J. Demsar, B. Podobnik, and D. Mihailovic, Phys. Rev. B **59**, 1497 (1999).

[28] C. J. Stevens, D. C. Smith, J. F. Ryan, B. Podobnik, and D. Mihailovic, Phys. Rev. Lett. **80**, 3665 (1998).

[29] C. J. Stevens, D. C. Smith, C. Chen, J. F. Ryan, B. Podobnik, D.

Mihailovic, G. A. Wagner, and J. E. Evetts, Phys. Rev. Lett. **78**, 2212 (1997).
[30] S. Shikii, T. Kondo, M. Yamashita, M. Tonouchi, M. Hangyo, M. Tani, and K. Sakai, Appl. Phys. Lett. **74**, 1317 (1999).
[31] Y. G. Zhao, J. J. Li, R. Shreekala, H. D. Drew, C. L. Chen, W. L. Cao, C. H. Lee, M. Rajeswari, S. B. Ogale, and R. Ranesh, Phys. Rev. Lett. **81**, 1310 (1998).
[32] A. Frenkel, F. Gao, Y. Liu, J. F. Whitaker, C. Uher, S. Y. Hou, and J. M. Phillips, Phys. Rev. B **54**, 1355 (1996).
[33] M. Hangyo, S. Tomozawa, Y. Murakami, M. Tonouchi, M. Tani, Z. Wang, K. Sakai, and S. Nakashima, Appl. Phys. Lett. **69**, 2122 (1996).
[34] C. Jaekel, H. G. Roskos, and H. Kurz, Phys. Rev. B **54**, R6889 (1996).
[35] R. C. Haddon, L. F. Schneemeyer, J. V. Waszczak, S. H. Glarum, R. Tycko, G. Dabbagh, A. R. Kortan, A. J. Muller, A. M. Mujsce, M. J. Rosseinsky, S. M. Zahurak, A. V. Makhija, F. A. Thiel, K. Raghavachari, E. Cockayne, and V. Elser, Nature (London) **350**, 46 (1991).
[36] M. S. Dresselhaus, G. Dresselhaus, and P. C. Eklund, *Science of Fullerenes and Carbon Nanotubes* (Academic Press, New York, 1996).
[37] Y. Liu, J. F. Whitaker, C. Uher, J.-L. Peng, Z. Y. Li, and R. L. Greene, Appl. Phys. Lett. **63**, 979 (1993).
[38] H. J. Zeiger (unpublished).
[39] A. F. Hebard, C. B. Eom, R. M. Fleming, Y. J. Chabal, A. J. Muller, S. H. Glarum, G. J. Pietsch, R. C. Haddon, A. M. Mujsce, M. A. Paczkowski, and G. P. Kochanski, Appl. Phys. A: Solids Surf. **57**, 299 (1993).
[40] A. F. Hebard, R. C. Haddon, R. M. Fleming, and A. R. Kortan, Appl. Phys. Lett. **59**, 2109 (1991).
[41] M. W. Zemansky and R. H. Dittman, *Heat and Thermodynamics*, 6th ed. (McGraw-Hill, New York, 1981).
[42] T. B. Norris, Opt. Lett. **17**, 1009 (1992).
[43] J. D. Kafka, M. L. Watts, and J. W. Pieterse, J. Opt. Soc. Am. B **12**, 2147 (1995).
[44] S. B. Fleischer, B. Pevzner, D. J. Dougherty, H. J. Zeiger, G. Dresselhaus, M. S. Dresselhaus, E. P. Ippen, and A. F. Hebard, Appl. Phys. Lett. **71**, 2734 (1997).
[45] S. D. Brorson, A. Kazeroonian, J. S. Moodera, D. W. Face, T. K. Cheng, E. P. Ippen, M. S. Dresselhaus, and G. Dresselhaus, Phys. Rev. Lett. **64**, 2172 (1990).
[46] M. Tinkham and J. Clarke, Phys. Rev. Lett. **28**, 1366 (1972).
[47] A. Schmid and G. Schoen, J. Low Temp. Phys. **20**, 207 (1974).
[48] Y. Iwasa, K. Tanaka, T. Yasuda, T. Koda, and S. Koda, Phys. Rev. Lett. **69**, 2284 (1992).
[49] L. Degiorgi, E. J. Nicol, O. Klein, G. Grüner, P. Wachter, S. M. Huang, J. Wiley, and R. B. Kaner, Phys. Rev. B **49**, 7012 (1994).
[50] M. Tinkham, *Introduction to Superconductivity* (McGraw-Hill, New York, 1996).
[51] G. Rickayzen, in *Superconductivity*, edited by R. D. Parks (Marcel Dekker, New York, 1969), Vol. I, Chap. 2.
[52] Philip B. Allen, Phys. Rev. Lett. **59**, 1460 (1987).
[53] Stuart D. Brorson, Ph.D. thesis, Massachusetts Institute of Technology, 1990.
[54] W. L. McMillan, Phys. Rev. **167**, 331 (1968).